

Three-dimensional functional magnetic resonance imaging of human brain on a clinical 1.5-T scanner

PETER VAN GELDEREN^{†‡}, NICK F. RAMSEY[§], GUOYING LIU[†], JEFF H. DUYN[¶], JOSEPH A. FRANK[¶], DANIEL R. WEINBERGER[§], AND CHRIT T. W. MOONEN[†]

[†]National Institutes of Health In Vivo Nuclear Magnetic Resonance Research Center, Biomedical Engineering and Instrumentation Program, National Center for Research Resources, Building 10, Room B1D-125, Bethesda, MD 20892; [§]Clinical Brain Disorders Branch, National Institute of Mental Health, National Institutes of Health, 2700 Martin Luther King, Jr., Avenue, S.E., Washington, DC 20032; and [¶]Laboratory Diagnostic Radiology Research Program, Office of Intramural Research, National Institutes of Health, Bethesda, MD 20892

Communicated by Robert G. Shulman, Yale University School of Medicine, New Haven, CT, April 17, 1995 (received for review January 30, 1995)

ABSTRACT Functional magnetic resonance imaging (fMRI) is a tool for mapping brain function that utilizes neuronal activity-induced changes in blood oxygenation. An efficient three-dimensional fMRI method is presented for imaging brain activity on conventional, widely available, 1.5-T scanners, without additional hardware. This approach uses large magnetic susceptibility weighting based on the echo-shifting principle combined with multiple gradient echoes per excitation. Motor stimulation, induced by self-paced finger tapping, reliably produced significant signal increase in the hand region of the contralateral primary motor cortex in every subject tested.

Mapping of human brain activity with positron emission tomography (PET) and single photon emission computed tomography (SPECT) is based on changes in metabolism or hemodynamics that accompany neuronal activation. It has been shown that similar information can be obtained with magnetic resonance imaging (1). In particular, functional magnetic resonance imaging (fMRI) methods based on blood oxygenation level-dependent (BOLD) (2, 3) contrast offer substantial advantages: minimal discomfort, no exposure to ionizing radiation, excellent spatial and temporal resolution, and straightforward registration with anatomical images. The BOLD effect is thought to arise because neuronal activity leads to hyperoxemia as increased local perfusion overcompensates for increased oxygen consumption.

fMRI is expected to be widely applied in the neurosciences, once a technique is available that permits imaging of the whole brain on standard available instruments. Most currently available fMRI methods involve echo planar imaging (EPI), which requires specialized hardware, or fast gradient echo techniques, and they involve repetitively scanning a single slice (two-dimensional) or a limited series of slices through the brain (4–14). While imaging of larger brain structures can be achieved by multislice or three-dimensional (3D) scanning methods, 3D methods are generally more efficient for imaging contiguous volumes and offer advantages in fMRI for correcting head motion (3D rotation and translation) between scans and for avoiding inflow effects. This paper presents an approach for 3D fMRI on conventional scanners, and it reports results of application in a simple motor activation study in 10 subjects. The reproducibility and selectivity of activation-induced signal changes were evaluated by using a simple and rigorous statistical analysis.

Conventional 3D gradient echo methods require prohibitively long acquisition times for fMRI since only one K -space line (K -space is the spatial Fourier transform of the image, the form in which the data are acquired) is collected for each rf

excitation pulse. The repetition time (TR, time between successive rf pulses) must be longer than the echo time (TE, time between excitation and echo), which in turn must be long for sufficient susceptibility (T_2^*) weighting. Recently, gradient echo techniques were introduced (15, 16) in which the echoes are shifted beyond the next rf pulse ($TE > TR$). This echo shifting leads to time-efficient T_2^* weighting. Initial attempts to use the echo shifting concept for 3D fMRI on clinical scanners were presented recently (17). Here, an approach is presented that combines echo shifting with multiple gradient echoes per rf excitation (PRESTO: principles of echo shifting with a train of observations), yielding faster and more reliable 3D functional images.

METHODS

fMRI. All studies were performed on a conventional 1.5-T GE/SIGNA scanner (General Electric) using the GE quadrature head coil and shielded gradients with maximum amplitude of $10 \text{ mT}\cdot\text{m}^{-1}$ and maximum slew rate of $17 \text{ T}\cdot\text{m}^{-1}\cdot\text{s}^{-1}$. Informed consent was obtained from healthy volunteers. The protocol was approved by the intramural review board of the National Institute of Mental Health.

The pulse sequence of 3D PRESTO, which is based on a recently described two-dimensional version (18), is given in Fig. 1. Additional gradient crushers of 2 ms before and 3 ms after the data acquisition period were used with $-3.75 \text{ mT}\cdot\text{m}^{-1}$ and $5 \text{ mT}\cdot\text{m}^{-1}$ strength, respectively, in all three principal directions. The additional gradient pulses were identical in each TR period and resulted in selection of gradient echoes shifted by a single TR period (16).

Each TR period (24 ms) contained five gradient echoes (Fig. 1). The T_2^* weighting varied from 29.6 ms for the first gradient echo in each TR period to 40.4 ms for the last echo. The optimal echo time is approximately equal to T_2^* (for brain tissue at 1.5 T, about 70 ms). However, at 35-ms echo time the BOLD T_2^* effect is already 80% of its maximum (19). Imaging of the whole superior brain down to the basal ganglia was achieved by selecting a 65-mm-thick axial slice. A data matrix of $64 \times 50 \times 24$ voxels (volume elements) was used in combination with a $240 \times 187.5 \times 90$ mm field of view, resulting in 3.75-mm isotropic resolution. The full width at half maximum, determined by the applied window function, was 4.5 mm isotropic.

K -space was split in five equal sections in the second dimension, each of which was encoded by using one of the five gradient echoes of each TR period, in linear order. The neighboring lines in this dimension, within each section, were

Abbreviations: 3D, three-dimensional; fMRI, functional magnetic resonance imaging; BOLD, blood oxygenation level-dependent; EPI, echo planar imaging; PRESTO, principles of echo shifting with a train of observations; TE, echo time; TR, repetition time; BA, Brodmann's area(s).

[‡]To whom reprint requests should be addressed.

The publication costs of this article were defrayed in part by page charge payment. This article must therefore be hereby marked "advertisement" in accordance with 18 U.S.C. §1734 solely to indicate this fact.

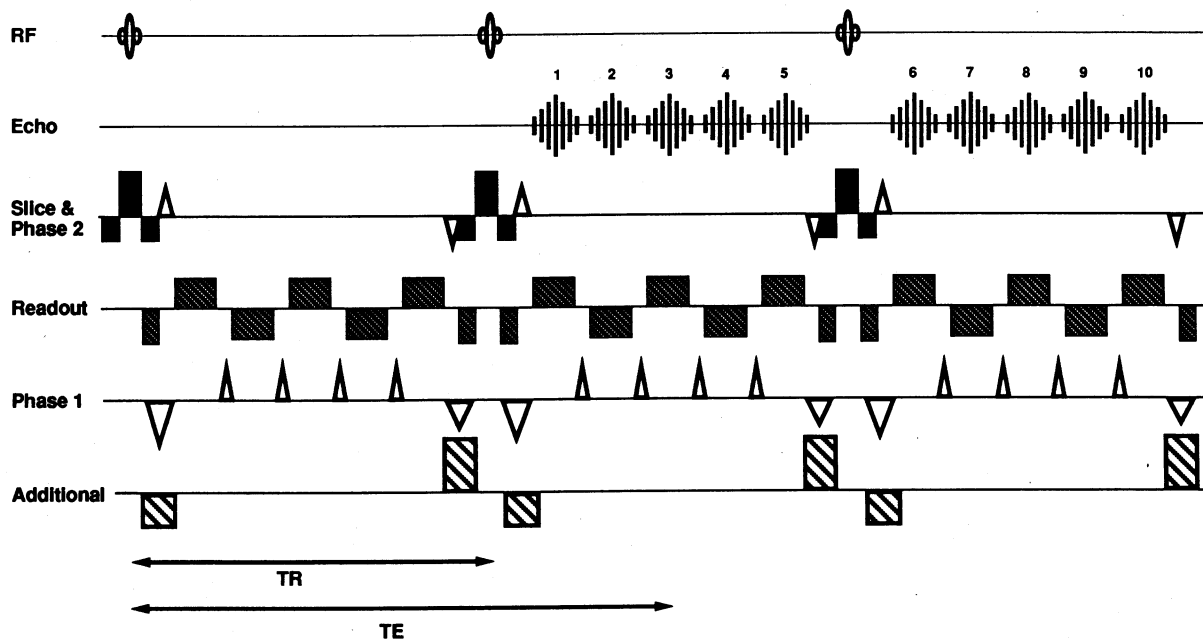


FIG. 1. Pulse sequence for 3D PRESTO, showing rf pulses, echoes, and gradient waveforms in three TR periods. The slice (selection), the readout, and the phase (encoding) gradients perform the basic imaging functions, with phase encoding in phase and slice directions for 3D imaging. All these waveforms are refocused in every TR period. The additional gradient waveform is added to all three principal gradient directions and serves to select the echoes shifted by one TR period (16). Therefore, the relative surface area of negative and positive additional gradient pulses is 1:2.

acquired in subsequent TR periods. Since PRESTO can be considered as a combination of echo-shifting and interleaved EPI, the PRESTO sequence also can give rise to susceptibility or chemical shift artifacts in the phase-encode dimensions. However, the severity of these artifacts is related to the time interval between first and last echo, which is substantially less in the PRESTO than a typical EPI echo train.

The sampling frequency was 32 kHz, and the total acquisition time for a 3D data set was 5.8 s. An rf flip angle of 11° was used, which was close to the calculated Ernst angle for grey matter [$\cos(\theta) = e^{-TR/T_1} \Rightarrow \theta = 14^\circ$, assuming $T_1 = 800$ ms]. rf phase spoiling was used (17).

Functional data were acquired in four blocks of 4 min each (alternating left and right hand between blocks), comprising 40 3D-scans. The subject switched between rest and finger tapping every 30 s, starting with rest. Five images (i.e., 3D volumes) were acquired during each period. Finger tapping was self-paced (2 Hz) and consisted of sequential thumb-to-digit opposition (order: 2, 3, 4, 5, 5, 4, 3, 2). The tapping periods were indicated to the subject by an assistant touching the leg, who also observed the performance of the subjects. Sessions were concluded with anatomical scans of the same volume [GE spin echo inversion recovery (IR), inversion delay = 800 ms, TR = 3000 ms, and TE = 16 ms]. Data were processed off-line on Sun-SPARC workstations (Sun Microsystems, Mountain View, CA) using IDL processing software (Research Systems, Boulder, CO). The first scan of each series of five was discarded, because the vascular response to neuronal activation exhibits a delay of a few seconds (5). The images from the two blocks with the same tapping hand were combined in one data set. All images were then registered to the first image of the data set (estimated error < 0.5 mm) to correct for small translations and rotations between scans, using a custom-written software program (20) based on a least-squares differences algorithm. The four images within each 30-s period were subsequently averaged, producing 16 images per data set. Each pair of images (one resting period and the following activation period) was converted to one difference image. The resulting eight difference images were subjected to statistical analysis.

Analysis. The difference images were analyzed on a voxel-by-voxel basis by means of a Z statistic adjusted for the total number of voxels by using a Bonferroni correction (voxels are virtually independent). For each voxel, average signal change and variance were calculated from the eight difference images. A pooled variance was obtained by averaging the voxel variances over the entire volume of brain tissue. A χ^2 statistic (voxel variance over pooled variance) was used to identify voxels with excessive variance at an α level of 0.01. A threshold was derived on the basis of the random Gaussian field model (21). A separate pooled variance was computed for these voxels. The number of voxels identified in this way was less than 1% of the total volume. A Z value was computed for each voxel as the product of the averaged voxel signal change times the square root of the number of on-off pairs (i.e., eight) divided by the pooled standard deviation. The Bonferroni corrected α

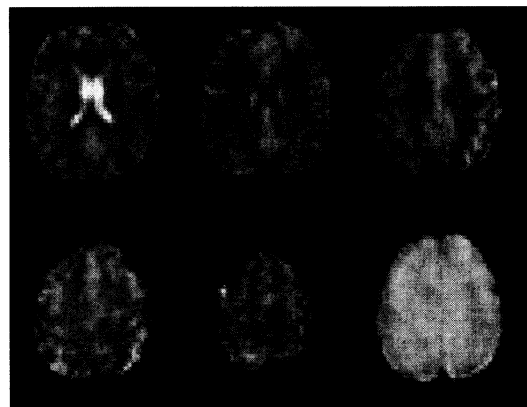


FIG. 2. Five axial slices of a 3D data set (slices 9, 11, 13, 15, and 17 of 24 slices), acquired with the 3D-PRESTO sequence, with excitation flip angle of 5° , and one (slice 13) from a 3D data set acquired with the flip angle used in the functional scans (11° , lower right). The images acquired with low flip angle show grey/white matter contrast due to spin density differences and illustrate the spatial fidelity of the image. For the higher flip angle, used for signal-to-noise purposes, this contrast is offset by T_1 relaxation differences.

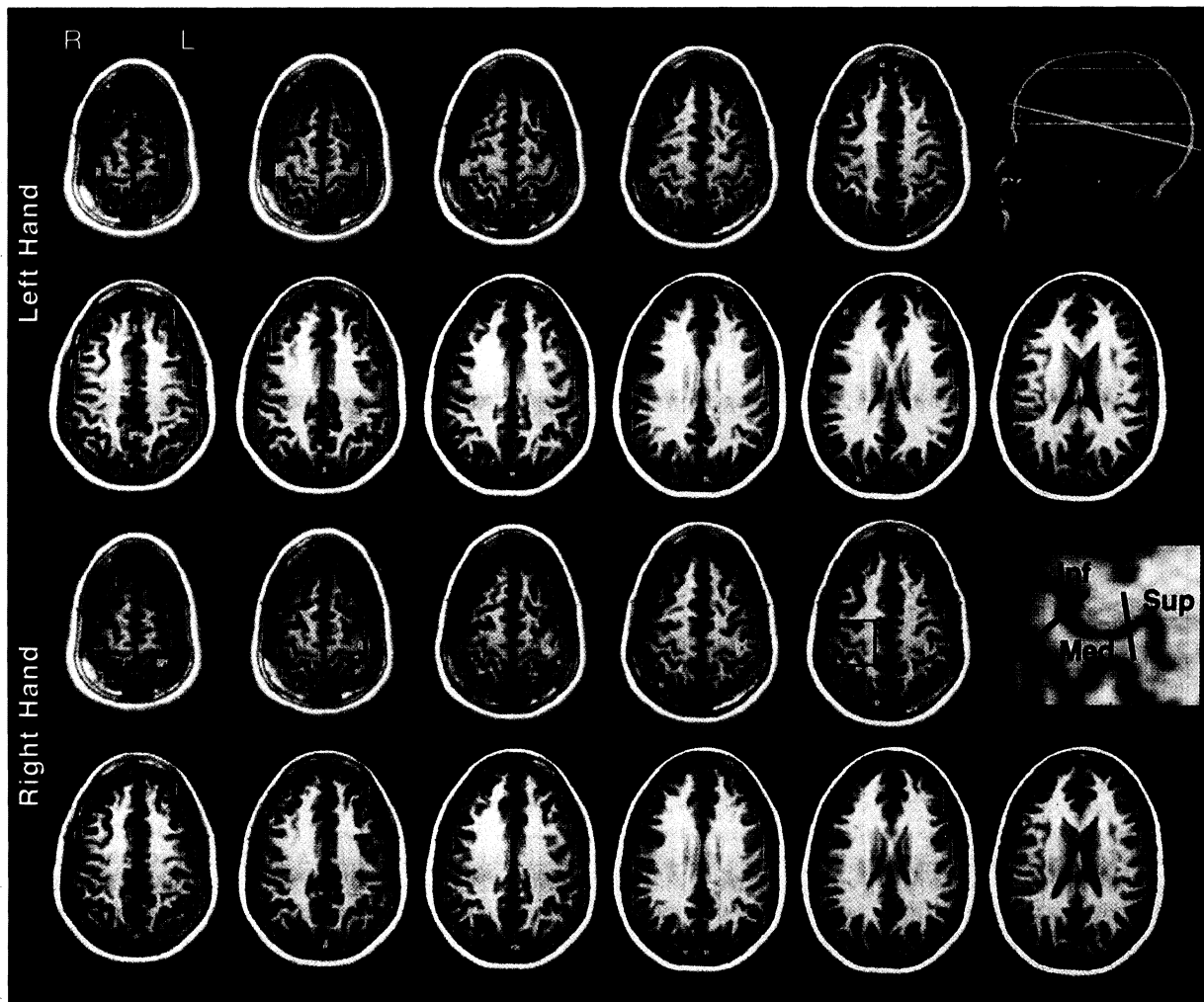


FIG. 3. Example of functional data obtained with the PRESTO technique (volunteer 1) overlaid on anatomical images. Shown are 11 slices of the 24-slice study. Sagittal slice shows location and angulation of the total volume. Note that the slice is tilted approximately -14° with respect to the anterior commissure–posterior commissure line. Yellow voxels represent a significant signal increase (see text). Blue voxels represent significant signal decrease, which in this case appeared only with the left-hand activation. All voxels have the dimensions of the nominal PRESTO image resolution (3.75 mm isotropic). The outer rim of a functional image is shown in yellow. The labeled enlargement outlined in red identifies regions mentioned in Fig. 4.

level was determined for each individual. The number of voxels in the brain was typically 12,000, resulting in an α level of 4.5×10^{-6} per voxel. All voxels with significant signal change (positive and negative, Z score ≥ 4.44 , omnibus α level 0.1 two-sided) were projected onto the anatomical images for structural localization (“activated” voxels). The anatomical maps were aligned to the first image of the functional data set by surface-to-surface registration.

RESULTS AND DISCUSSION

The image quality of the PRESTO sequence is shown in Fig. 2 for two flip angles. Signal-to-noise ratio (average signal over average background noise in the acquisition direction) was 120–150 in the functional scans. The stability was 0.8–1.2% (average standard deviation over eight difference volumes relative to average of volumes).

An example of the functional studies is displayed in Fig. 3. Results of the functional studies are summarized in Table 1. Significant signal changes were found selectively in the region around the contralateral central sulcus [Brodmann’s areas (BA) 3 and 4], for both hands in all tested subjects. These voxels were located predominantly in parts of the primary motor and sensory areas on the medial genu (22) of the central sulcus [Fig. 4; EF-b-12 to EF-bc-3 in Talairach coordinates

(23)]. The location of the center of each voxel determined the assignment to either motor or sensory cortex. The results are in agreement with earlier reports on functional topography (24–32). The recently reported increase in ipsilateral hemispheric activity for the nondominant hand (13) was not confirmed in this study.

Additional findings are presented in Table 2, summarizing voxels in the premotor area (around the precentral sulcus, lateral aspect of BA 6), anterior superior parietal cortex (around the postcentral sulcus, BA 2, 5, and 40), and the supplementary motor area (ref. 25; interhemispheric aspect of BA 6). The superior parietal cortex showed predominantly contralateral activation; the premotor area showed no discernible pattern of lateralization. In three of the volunteers, activation was found in the right posterior superior parietal cortex (BA 7), for both left- and right-hand tasks. These areas are known to be involved in voluntary motor activity (24–32).

The magnitude of the signal increase in activated voxels ranged from 1.6% to 3% (mean 2.36%, standard deviation 0.39%), corresponding with previous results using EPI techniques at 1.5 T (4). The number of activated voxels varied considerably between volunteers. No correlation was found between the extent of activation and the pooled standard deviation. The number of activated voxels for left and right finger tapping within one volunteer showed a strong correla-

Table 1. Sum of voxels with significant activation in primary motor and sensory cortices in each of the 10 volunteers

Vol- unteer	HS	No. of voxels									
		Left hand					Right hand				
		Motor		Sensory			Motor		Sensory		
R	L	R	L	Total	R	L	R	L	Total		
1	0.8	13	—	13	—	53	—	11	—	6	34
2	-0.8	6	—	—	—	22	—	4	—	1	16
3	0.6	16	—	22	—	104	—	18	—	9	93
4	-1.0	9	7	4	6	179	2	19	—	16	125
5	0.8	29	2	9	—	86	—	5	—	4	16
6	1.0	24	2	20	—	161	2	12	1	5	97
7	0.7	5	1	4	—	44	1	2	—	1	13
8	1.0	1	—	2	1	65	—	2	—	—	3
9	0.5	12	—	3	—	29	—	2	—	—	5
10	0.8	5	—	3	—	15	—	3	—	—	14

Hand score (HS) is the result of the Edinburgh handedness test (+1 is right-handed). "Left hand" and "Right hand" refer to the hand used for the tapping procedure; R and L refer to right and left hemispheres, respectively. Numbers for the motor and sensory cortex are the total number of voxels found immediately anterior and posterior to the central sulcus, respectively. Total is the total number of activated voxels in the whole scanned volume (approximately 12,000 voxels).

tion ($\rho = 0.9$; Table 1). Significant signal decrease was detected in 21% of the total number of significant voxels. These were located predominantly in the lower slices, in particular temporal lobes and orbital frontal cortex. The interpretation of these voxels in BOLD contrast methods remains unclear.

Recent fMRI studies have raised the issue that signal changes may reflect vascular contributions through the inflow phenomenon (33). Vascular water excited during scanning of one plane may give rise to signal changes in another plane when transported within the T_1 relaxation time. However, inflow effects in 3D studies are minimal under experimental conditions similar to those used in this study (17).

Magnetic susceptibility effects may be enhanced around large veins draining an extended activated region. Larger vessels may therefore also contribute to the signal changes detected with BOLD-based fMRI methods. The present findings suggest that signal changes are not dominated by draining veins for several reasons. Activated voxels were mainly located in grey matter, and they form clusters much larger than the diameter of sulcal veins. These clusters corresponded well with known functional anatomy. Furthermore, in eight of the studies the activated region (in the sensory and motor area) did

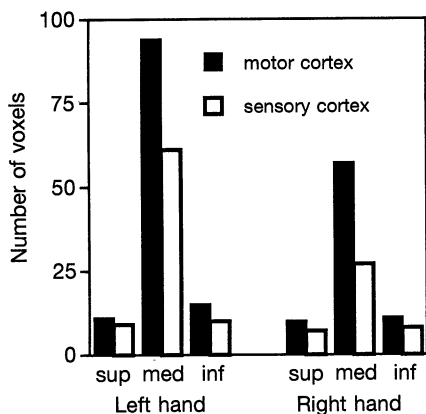


FIG. 4. Distribution of activation on motor and sensory cortices. Bars show number of voxels, summed over all volunteers. Activation is concentrated around the medial genu (med), believed to be the hand region of the cortex, with some voxels in the inferior and superior genua (inf and sup). The regions are indicated in Fig. 3.

Table 2. Sum of activated voxels in the supplementary motor areas (SMA), the premotor areas (PM), and the anterior superior parietal cortex (ASP)

Vol- unteer	No. of voxels									
	Left hand					Right hand				
	SMA	PM		ASP		SMA	PM		ASP	
R	L	R	L	Total	R	L	R	L	Total	
1	4	1	—	—	—	—	—	—	6	—
2	—	—	1	4	—	—	—	1	—	2
3	21	8	8	17	—	29	—	14	—	15
4	12	17	5	7	4	31	9	6	12	15
5	2	5	—	22	3	—	—	—	—	7
6	6	3	6	32	14	2	8	3	14	7
7	—	—	—	1	—	4	—	1	—	—
8	—	—	2	2	—	—	—	—	—	—
9	7	1	—	2	—	—	—	—	—	—
10	—	3	—	1	—	3	—	5	1	1

Other abbreviations are explained in the legend of Table 1.

not extend to the superior surface of the brain where the major draining veins are located.

CONCLUSION

The results confirm that 3D PRESTO is an effective and reliable approach for mapping of brain activity in a simple motor stimulation procedure using a conventional magnetic resonance instrument and a standard head coil. The main advantages of the 3D PRESTO method are (i) coverage of a large part of the human brain in a short imaging time, (ii) straightforward correction of interscan motion, and (iii) elimination of confounding inflow effects.

The authors thank Geoffrey Sobering and Yoseph Shiferaw for technical assistance and Philippe Thévenaz for making his 3D registration software available to us and providing excellent advice. We acknowledge Bob Rawlings for help in the design of the statistical parametric mapping. This work was performed in the In Vivo Nuclear Magnetic Resonance Research Center at the National Institutes of Health.

- Belliveau, J. W., Kennedy, D. N., McKinstry, R. C., Buchbinder, B. R., Weisskoff, R. M., Cohen, M. S., Vevea, J. M., Brady, T. J. & Rosen, B. R. (1991) *Science* **254**, 716–719.
- Ogawa, S., Lee, T. M., Nayak, A. S. & Glynn, P. (1990) *Magn. Reson. Med.* **14**, 68–78.
- Ogawa, S., Lee, T. M., Ray, A. R. & Tank, D. W. (1990) *Proc. Natl. Acad. Sci. USA* **87**, 9868–9872.
- Kwong, K. K., Belliveau, J. W., Chesler, D. A., Goldberg, I. E., Weisskoff, R. M., Poncelet, B. P., Kennedy, D. N., Hoppel, B. E., Cohen, M. S., Turner, R., Cheng, H.-M., Brady, T. J. & Rosen, B. R. (1992) *Proc. Natl. Acad. Sci. USA* **89**, 5675–5679.
- Ogawa, S., Tank, D. W., Menon, R., Ellermann, J. M., Kim, S.-G., Merkle, H. & Ugurbil, K. (1992) *Proc. Natl. Acad. Sci. USA* **89**, 5951–5955.
- Turner, R., Jezzard, P., Wen, H., Kwong, K. K., LeBihan, D., Zeffiro, T. & Balaban, B. (1993) *Magn. Reson. Med.* **29**, 277–279.
- Bandettini, P. A., Wong, E. C., Hinks, R. S., Tikofsky, R. S. & Hyde, J. S. (1992) *Magn. Reson. Med.* **25**, 390–397.
- Blamire, A. M., Ogawa, S., Ugurbil, K., Rothman, D., McCarthy, G., Ellermann, J. M., Hyder, F., Rattner, Z. & Shulman, R. G. (1992) *Proc. Natl. Acad. Sci. USA* **89**, 11069–11073.
- McCarthy, G., Blamire, A. M., Puce, A., Nobre, A. C., Bloch, G., Hyder, F., Goldman-Rakic, P. & Shulman, R. G. (1994) *Proc. Natl. Acad. Sci. USA* **91**, 8690–8694.
- Frahm, J., Bruhn, H., Merboldt, K. & Hänicke, W. (1992) *J. Magn. Reson. Imaging* **2**, 501–505.
- Connelly, A., Jackson, G. D., Frackowiak, R. S. J., Belliveau, J. W., Vargha-Khadem, F. & Gadian, D. G. (1993) *Radiology* **188**, 125–130.
- Menon, R. S., Ogawa, S., Tank, D. W. & Ugurbil, K. (1993) *Magn. Reson. Med.* **30**, 380–386.

13. Kim, S.-G., Ashe, J., Hendrich, K., Ellermann, J. M., Merkle, H., Ugurbil, K. & Georgopoulos, A. P. (1993) *Science* **261**, 615–617.
14. Schneider, W., Noll, D. C. & Cohen, J. D. (1993) *Nature (London)* **365**, 150–153.
15. Moonen, C. T. W., Liu, G., van Gelderen, P. & Sobering, G. S. (1992) *Magn. Reson. Med.* **26**, 184–189.
16. Liu, G., Sobering, G. S., Olson, A. W., van Gelderen, P. & Moonen, C. T. W. (1993) *Magn. Reson. Med.* **30**, 68–75.
17. Duyn, J. H., Mattay, V. S., Sexton, R., Sobering, G. S., Barrios, F. A., Liu, G., Frank, J. A., Weinberger, D. R. & Moonen, C. T. W. (1994) *Magn. Reson. Med.* **32**, 150–155.
18. Liu, G., Sobering, G. S., Duyn, J. H. & Moonen, C. T. W. (1993) *Magn. Reson. Med.* **30**, 764–768.
19. van Gelderen, P., Duyn, J. H., Liu, G. & Moonen, C. T. W. (1994) *Proc. Indian Acad. Sci. Chem. Sci.* **106**, 1617–1624.
20. Unser, M., Aldroubi, A. & Gerfen, C. R. (1993) *Math. Imaging* **2034**, 160–166.
21. Worsley, K. J. (1995) *Adv. Appl. Probab.* **26**, 13–42.
22. Ono, M., Kubik, S. & Abernathy, C. D. (1990) *Atlas of the Cerebral Sulci* (Thieme, Stuttgart), p. 36.
23. Talairach, J. & Tournoux, P. (1988) *Co-Planar Stereotaxic Atlas of the Human Brain* (Thieme, Stuttgart).
24. Carpenter, M. B. (1976) *Human Neuroanatomy* (Williams & Wilkins, Baltimore), 7th Ed., p. 579.
25. Penfield, W. & Boldrey, E. (1937) *Brain* **60**, 389–443.
26. Penfield, W. & Welch, K. (1951) *Arch. Neurol. Psychiatry* **66**, 289–317.
27. Roland, P. E., Larsen, B., Lassen, N. A. & Skinhøj, E. (1980) *J. Neurophysiol.* **43**, 118–136.
28. Fox, P. T., Fox, J. M., Raichle, M. E. & Burde, R. M. (1985) *J. Neurophysiol.* **54**, 348–369.
29. Colebatch, J. G., Dreiber, M.-P., Passingham, R. E., Friston, K. J. & Frackowiak, R. S. J. (1991) *J. Neurophysiol.* **65**, 1392–1401.
30. Deiber, M.-P., Passingham, R. E., Colebatch, J. G., Friston, K. J., Nixon, P. D. & Frackowiak, R. S. J. (1991) *Exp. Brain Res.* **84**, 393–402.
31. Grafton, S., Woods, R. & Mazziotta, J. C. (1993) *Exp. Brain Res.* **95**, 172–176.
32. Rumeau, C., Tzourio, N., Marayama, N., Peretti-Viton, P., Levrier, O., Joliot, M., Mazoyer, B. & Salamon, G. (1994) *Am. J. Neuroradiol.* **15**, 567–572.
33. Duyn, J. H., Moonen, C. T. W., de Boer, R. W., van Yperen, G. H. & Luyten, P. R. (1994) *NMR Biomed.* **7**, 83–88.